waste

MDPI

Article

Collection Efficiency of Cyclone Separators: Comparison between New Machine Learning-Based Models and Semi-Empirical Approaches

Edoardo Bregolin [1,*], Piero Danieli [2] and Massimo Masi [2]

[1] Department of Industrial Engineering, University of Padova, Via Venezia 1, 35131 Padova, Italy
[2] Department of Management and Engineering, University of Padova, Stradella S. Nicola 3, 36100 Vicenza, Italy; piero.danieli@unipd.it (P.D.); massimo.masi@unipd.it (M.M.)
* Correspondence: edoardo.bregolin@phd.unipd.it

Abstract: Cyclones are employed in many waste treatment industries for the dust collection or abatement purposes. The prediction of the dust collection efficiency is crucial for the design and optimization of the cyclone. However, this is a difficult task because of the complex physical phenomena that influence the removal of particles. Aim of the paper is to present two new meta-models for the prediction of the collection efficiency curve of cyclone separators. A Backpropagation Neural Network (BPNN) and Support Vector Regression (SVR) models were developed using Python environment. These were trained with a set of experimental data taken from the literature. The prediction capabilities of the models were first assessed by comparing the estimated collection efficiency for several cyclones against the corresponding experimental data. Second, by comparing the collection efficiency curves predicted by the models and those obtained from classic models available in the literature for the cyclones included in the validation dataset. The BPNN demonstrated better predictive capability than the SVR, with an overall mean squared error of 0.007 compared to 0.015, respectively. Most important, a 40% to 90% accuracy improvement of the literature models predictions was achieved.

Keywords: cyclone; efficiency; machine learning; dust treatment

Citation: Bregolin, E.; Danieli, P.; Masi, M. Collection Efficiency of Cyclone Separators: Comparison between New Machine Learning-Based Models and Semi-Empirical Approaches. *Waste* **2024**, *2*, 240–257. https://doi.org/10.3390/waste2030014

Academic Editor: Catherine N. Mulligan

Received: 2 July 2024
Revised: 9 July 2024
Accepted: 15 July 2024
Published: 18 July 2024

1. Introduction

Cyclone separators are widely used for the control of dust-laden air in different industrial sectors [1,2]. In metal scrap recycling process they are employed for the collection of the dust coming from the shredding process of the metallic waste. Frolov et al. [3] employed two cyclone separators for the exhaust gas cleaning system in the recycling process of printed circuit boards. Cyclones are known for their simple geometry, low maintenance requirements and ability to operate under extreme conditions of high pressure and temperature. The collection mechanism is based on the centrifugal forces generated by the swirling flow of the gas within the cyclone body [4,5]. The heavier and coarser particles, which have a greater inertia than the smaller and lighter ones, are transported downstream and therefore collected at the bottom of the machine. The cyclone performance is mainly determined by the gas pressure drop and the overall collection efficiency (η_c). The latter is defined as the amount of dust that is separated by the cyclone compared to that which entered the machine. Accordingly, the particle collection efficiency $\eta(D_p)$ is the mass fraction of separated particles with dimension D_p. The overall collection efficiency is used as an indicator of cyclone performance for the most of industrial applications. Another commonly used performance parameter is the cut-off diameter (D_{50}), which is the diameter of the particle that is separated with a 50% efficiency. Although these two parameters are largely utilized, the collection capability of cyclone separators is best described by the collection efficiency curve, which defines the collection efficiency for each size interval of

the treated particles [6,7]. The collection efficiency curve is essential for the description of the cyclone behaviour, especially when the processed particles have a size distribution, which happens in most of the industrial applications. The collection efficiency depends on some parameters that can be rather easily measured, such as geometrical dimensions of the cyclone or the physical properties of the particles carried by the gas. On the other hand, other influencing phenomena, such as the particle-wall and particle-particle interactions, are difficult to be characterized and make the prediction of the dust collection efficiency a complex task. In this context, a model that accurately predicts the collection efficiency curve on the basis of the cyclone geometry and process parameters is crucial for the optimal design of the machine. The scientific literature reports several semi-empirical models for the prediction of the particles collection efficiency of cyclone separators. Two classic semi-empirical approaches, namely the static particle approach and the timed flight approach [7], rely both on physics correlations and empirical data. Examples of the static particle approach are presented by Stairmand [8], Barth [9], Iozia et al. [10], while examples of the timed flight approach are reported by Lapple [11], Leith & Licht [12], Clift et al. [13]. Other authors developed models using an hybrid approach lying in between the two (Dietz [14], Mothes et al. [15], Li & Wang [16]). The previously mentioned models, while offering a practical approach to predict the cyclone collection efficiency, have demonstrated to be limited. In their study, Mumcu et al. [17] examined the capability of semi-empirical models in predicting the cut-off diameter of several experimental cyclones. The accuracy of the predictions varied significantly depending on the geometrical and process parameters of the examined cyclones, revealing a mean error between the 2% and 50%. Also, statistical models exploiting multi-linear regression were suggested by many authors. Examples are provided by Zhao [18], Iozia et al. [19] who predicted the collection efficiency curve with a mean error lower than that of the classic semi-empirical methods (2–20%). At present, CFD simulations are recognized as the most powerful tool for the prediction of the cyclones' collection efficiency. Several studies from the literature [20–23] compared the collection efficiencies derived from simulated cyclones with the corresponding experimental data, proving a mean error between the 1% and 4%. Despite the significant predictive capabilities of CFD models for cyclone performance, it is important to note that their development is encumbered by complexity. Furthermore, achieving reliable results necessitates a high computational cost.

Recently, machine learning (ML) methods have gained significant interest in practical engineering [24]. Many researchers have exploited different types of artificial neural networks (ANN) to support the design of cyclone separators. In this research field, three types of ANNs are reported: (i) Physics-Informed Neural Networks (PINN), which use physical laws to guide their learning process, (ii) Backpropagation Neural Networks (BPNN), that learn by adjusting their parameters based on the error in their predictions, (iii) Radial Basis Function Neural Networks (RBFNN), which employ specific functions to approximate any given input function or data [25]. Several studies utilized ANNs to predict the flow field and pressure drop of cyclone separators. Queiroz et al. [26] proposed a model based on PINN for the prediction of the velocity and pressure fields of a cyclone separator with different operating conditions. Elsayed et al. [27], Zhao et al. [28] developed a RBFNN that derives the pressure drop of cyclone separator on the basis of the geometrical sizes and process parameters. Other contributions employed ANNs to investigate the impact of the cyclone geometrical dimensions and process parameters on the collection efficiency. Brar et al. [29] suggested the use of a RBFNN model as a cyclone surrogate to study the effect of process parameters (cyclone inlet area, inlet vertical position, air flow rate) on the collection efficiency. Elsayed et al. [30] investigated the impact of four geometrical parameters (cyclone inlet height, inlet width, vortex finder diameter and total height) on the cyclone cut-off diameter using a meta-model based on a RBFNN. The latter showed a zero mean squared error in fitting the cyclone experimental data and was used to determine an optimized cyclone geometry. Other research approaches use ANNs for the prediction of the cyclone collection efficiency. Le et al. [31] utilised the regression capability of a BPNN

in combination with a coarse-grid CFD model of the cyclone to predict the cut-off diameter. In order to achieve a low computational cost, the BPNN was used to calculate a correction coefficient for the cut-off diameter value obtained with the coarse-grid CFD model. This hybrid BPNN-CFD model showed a good prediction accuracy, with a mean error ranging between 1% and 5% of the experimental cut-off diameters. Tang et al. [32] developed a cyclone meta-model based on a BPNN for estimating the overall separation efficiency of cyclones. The BPNN meta-model demonstrated to be capable of predicting the overall collection efficiency, with a mean error ranging between 0.2% and 3.8%.

Other works from literature employed support regression vector (SVR) models for cyclone optimization. Zhao [33] developed a SVR model to predict the cyclone pressure drop coefficient (PDC) on the base of cyclone dimensions. The model demonstrated to give better forecasts of the cyclone pressure drop in comparison to semi-empirical and statistical models. Deng et al. [34] proposed a hybrid CFD-support vector machine (SVM) model for the optimization of the guide vanes of an axial cyclone separator. The hybrid approach demonstrated higher accuracy and lower computational cost than the original CFD model in predicting the effects of guide vanes' geometry on cyclone performance. Zhang et al. [35] modelled the collection efficiency of a cyclone separator through an SVR-based algorithm. The developed model showed better predictive capability of the overall collection efficiency of the experimental cyclone in comparison with semi-empirical models.

From this literature overview, it appears that models based on statistical methods are better than semi-empirical models in predicting the cyclone collection efficiency, but still not very accurate. As far as ML-based models are concerned, they promise to be more accurate than the others, even though the available ones have focused only on the prediction of the cut-off diameter or the overall collection efficiency. The novelty of this work is to present for the first time two ML-based models, a BPNN model and a SVR model, for the prediction of cyclone efficiency curve in the entire range of dimensions of the ingested particles. Their predictive capabilities are assessed against experimental measurements and finally compared with those of classical methods. The original contribute of this study is to present simple models that can be replicated and used as a tool to predict the cyclones collection efficiency. The paper includes the training, validation and testing dataset of the experimental cyclones collected from the literature, which can be used to recreate the BPNN and SVR models. Moreover, it includes all weights and biases required to replicate the present meta-model without repeating the BPNN training process (which can be found in the Supplementary Materials).

2. Materials and Methods

The first of the following subsections presents a brief description of a general BPNN based meta-model; the second describes the BPNN structure considered in this work; the third and fourth presents a general description of SVR models and the one developed in the present work, respectively; subsequent five and six present the training and the experimental datasets for the models validation; the seventh provide insights on the semi-empirical and statistical models selected for the comparison with the present models.

2.1. Backpropagation Artificial Neural Networks

The structure on which ANNs working principle is based tries to emulate the connections between the neurons of a human brain. In ANNs, the nodes are able to learn complex relationships between the received input and output data to perform classification and regression tasks [36,37]. BPNNs are a type of supervised ANN, which learns from labelled data by adjusting the connections' weights between the nodes based on the errors it makes in predictions [38]. What distinguishes BPNNs, and in general ANNs, from the other regression models is their ability to capture non-linear relations between the input and output variables, thus leading to very accurate predictions. To do that, the BPNN consists of an input layer, a matrix of nodes referred as "hidden layers", and an output layer (McCulloch & Pitts [39]). The input layer consists of a set of nodes $[X_1, \ldots, X_n]$ with n

equal to the number of input variables, while each hidden layer comprises a vector of fully connected nodes. Each i-th node of the j-th hidden layer allows calculating an output $z_{i,j}$, which is the sum of the weighted contributions from all the previous layer nodes multiplied by a non-linear activation function $\varphi(z)$:

$$z_{i,j} = \varphi(z) * \left(\sum_{i=1}^{n} \left(w_{i,j} * z_{i,j-1}\right) + b_{i,j}\right) \quad (1)$$

where $w_{i,j}$ is a weight parameter and $b_{i,j}$ is a bias. Examples of activation functions $\varphi(z)$ are the logistic sigmoid, the ReLu and the hyperbolic tangent [40]. The nodes of the j-th hidden layer are fully connected to those of the succeeding j + 1-th hidden layer, which give $z_{i,j+1}$ as outputs. This is valid for all the hidden layers included in the BPNN structure. To make predictions, the BPNN must be trained with a set of labelled data (set of known input-output data). The aim of the training process is to find the values of the weights that minimise the error between the output of the network and the corresponding labelled values. The learning process is composed of two phases: first, the BPNN is trained using the majority of the dataset and second, the remaining data are utilized for the BPNN validation and testing. The validation is performed simultaneously with the training of the BPNN to avoid overfitting, which would take to a low generalization ability of the network. Instead, the testing is used to verify the network's capability to predict new data that was not included in the training process.

2.2. Proposed BPNN Model of the Cyclone

The BPNN model proposed in the present study aims to predict the particles collection efficiency of the cyclone $\eta(D_p)$, defined in Equation (2).

$$\eta(D_p) = \frac{M_{out} \cdot f_{out}(D_p)}{M_{in} \cdot f_{in}(D_p)} \quad (2)$$

For the prediction of the particles collection efficiency, the inputs of the BPNN-based meta-model are the geometrical variables and process parameters of cyclones. The present neural network is composed by an input layer of 7 variables (see Equation (7)) in accordance with the parameters that allows calculating the cyclone efficiency. The core structure is made by 3 hidden layers, each of these with 15 nodes (Figure 1a). The number of hidden layers and of the corresponding nodes are defined using trial and error criteria on the base of the dimension of the training dataset and number of independent input variables. The reported number of hidden layers and nodes for each layer are those that gave the best results in predictions with the lowest computational cost. The output layer consists of a single node since this BPNN works as a regression model that predicts one single value of the collection efficiency for a precise set of parameters. BPNN was chosen to make the regression of the cyclone experimental data for the prediction of the collection efficiency due to its ability to handle complex relationships and nonlinearities in the data. Unlike PINNs (Physics-Informed Neural Networks) and RBFNNs (Radial Basis Function Neural Networks), BPNNs can effectively learn intricate patterns without relying on explicit equations or assumptions.

The BPNN was trained with a set of experimental data derived from the literature (see Section 2.5). According to the dataset size and model complexity, the available dataset was divided into a training set and a validation-testing set including 80% and 20% of the samples, respectively (Figure 1b). For any training process, several characteristic hyperparameters must be defined. These are: (i) the training batch size which is the number of samples from the training dataset that propagate through the neural network before the model weights are updated (ii) the number of epochs that is the number of times that the model updates the values of the weights during the training process (iii) the optimization algorithm which determines the values of the weights ($w_{i,j}$ in Equation (1)) by minimizing the mean squared error between the outputs and the training labelled data (iv) the activation function that introduces non-linearity into the network (see Equation (1)). The choice of the

hyperparameters strongly affect the learning process and the predictive capability of the BPNN. Different combinations of number of epochs and batch size were determined on the base of the train loss curve. The optimization algorithms and activation functions that gave lower train losses were chosen for the study of the different combinations. Accordingly, multiple training processes were conducted considering various combinations of these parameters (grid search [41]), until satisfactory values of low mean train error (MTE), low mean validation error (MVE) and high mean testing accuracy (MTA) were found. The MTE and MVE are defined as the average of the training and validation losses, while the MTA is derived from the average absolute deviation between the experimental and the predicted value during testing, defined as:

$$\mathrm{MTA} = 1 - \frac{1}{n}\left(\sum_{i=1}^{n} \frac{\left|Y_{test}^{i} - Y_{pred}^{i}\right|}{Y_{test}^{i}}\right) \quad (3)$$

The prediction capability of the BPNN-based meta model was evaluated against experimental data available from the literature (See Section 2.6) and also compared to those of classic methods considering the mean squared error between the experimental and the predicted value:

$$E^2 = \frac{1}{n}\sum_{i=1}^{n}\left(Y_{exp}^{i} - Y_{pred}^{i}\right)^2 \quad (4)$$

The BPNN model has been developed in the Python environment through Keras library from Tensorflow open-source [42].

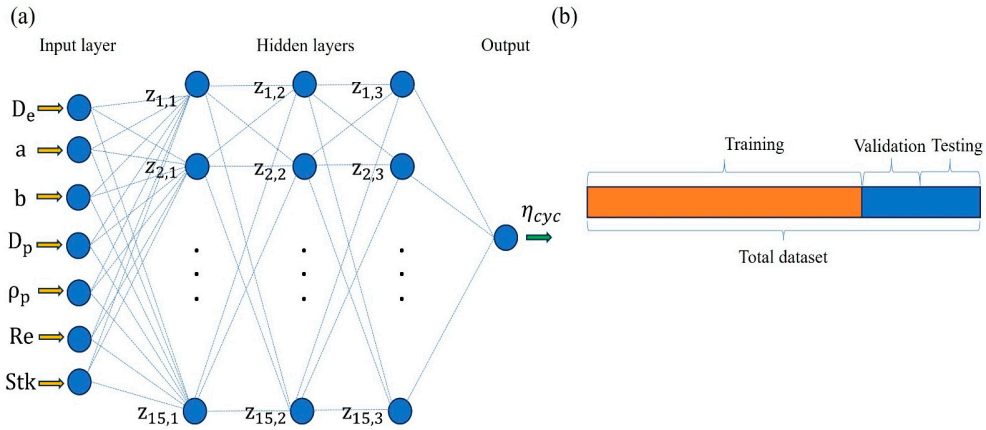

Figure 1. (**a**) Structure of the present BPNN (**b**) Split of the experimental dataset.

2.3. Support Vector Regression Model

Support Vector Regression (SVR) is a type of supervised machine learning model based on Support Vector Machines (SVM) and is particularly suited for regression tasks [43]. The SVR models approximate the relationship between input and output data by identifying a regression function that accurately interpolates the data points in a high-dimensional space. First, input data are transformed into a high-dimensional space using a kernel function [44]. An optimization algorithm is used to find an hyperplane, which is the regression function f(**x**) in the high-dimensional space, that fit the input data by minimizing the error between them and the predicted values. During the optimization problem a tolerance ε is used, where predictions' deviations of less than that are considered acceptable, in order to reduce the model complexity. The support vectors are the bounds of the tolerance zone, which determines the position and orientation of the regression function in the high-dimensional space. Mathematically, the regression function f(**x**) can be written as [43]:

$$f(\mathbf{x}) = \mathbf{w}^T\mathbf{x} + b \quad (5)$$

where **w** is the vector of the weights, **x** is the input vector in the M-dimensional space (**w**,**x**$\in \mathbb{R}^M$), b is the bias term. The optimization problem consists in finding the weights and biases by minimizing the following error function:

$$f_{err} = \frac{1}{2}\|\mathbf{w}\|^2 + C\sum_{i=1}^{n}(\xi_i) \quad (6)$$

The first term represents the weights vector's norm, minimizing that ensure to obtain a simple model with a regression function that is as flat as possible. The second term represents the deviations of the predicted values from the actual ones that exceed the tolerance margin ε by a value ξ_i, defined as the slack variables. C is a regularization parameter that determines a balance between the minimization of the two terms [45].

A mono-dimensional linear SVR is represented as an example in Figure 2, where the optimal regression function (optimal hyperplane, blue line) is between the two support vectors within the tolerance range (orange lines).

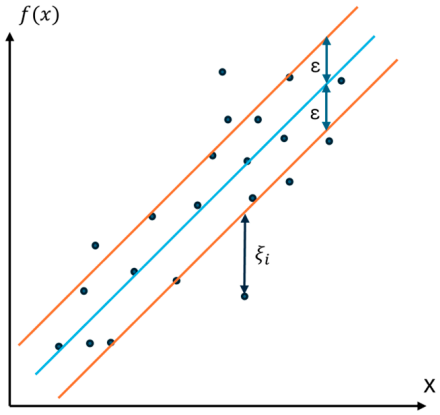

Figure 2. Example of a mono-dimensional linear SVR.

Compared to BPNNs, SVR models are constituted of simpler structure with less hyperparameters to be tuned for the training procedure. This leads to a lower effort in the hyperparameter optimization stage resulting in smaller computational cost of the model. Generally, SVR models can better handle overfitting during training in comparison to BPNNs [46]. This is due to the margin of tolerance ε and regularization parameter C, which enhance the generalization capability of the model rather than attempting to fit every single data point. On the other hand, BPNNs can better capture the non-linear relationships between input-output data than SVR models [47]. In particular, BPNNs tends to perform better than SVR when dealing with large datasets. This is correlated to the BPNNs' deep layered structure, which interconnected nodes can learn intricate patterns between data. Accordingly, the dimension of the BPNN network can be adapted to increase the model capacity to deal with complex datasets.

2.4. Present SVR Model

The present SVR model was developed in Python environment through the Sci-kit learn library [48]. As with the BPNN model, different combinations of hyperparameters have been tested in order to obtain a model with the maximum predictive capability. These are (i) the kernel function, which transform the input data into a higher-dimensional space, (ii) the regularization parameter C, that controls the trade-off between minimizing the norm of the weight vector and the total error outside the epsilon margin, (iii) the tolerance ε, which determines the range of acceptable solutions from the model predictions during training. The cyclone experimental dataset was split into training (80%) and testing (20%). The SVR with a certain combination of hyperparameters was evaluated with the mean train error (MTE) and mean testing accuracy (MTA) (see Equation (3)).

2.5. Dataset for the Training and Testing of BPNN

The geometry of the tangential-inlet reverse-flow cyclone considered in this study is reported in Figure 3.

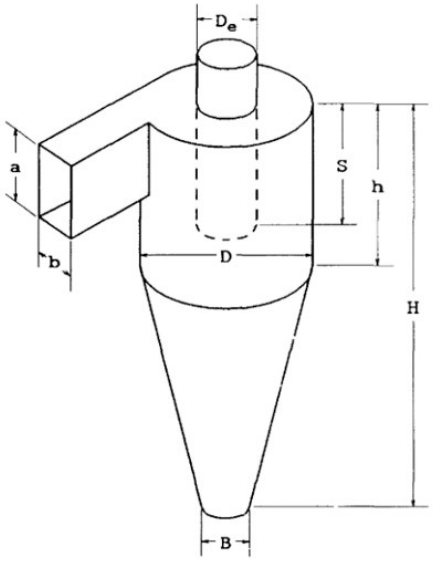

Figure 3. Cyclone geometry.

Assuming that the gas flow is incompressible, low particle load, no particle agglomeration and negligible effect of the wall roughness; the particles collection efficiency of the cyclone can be defined as a function of:

$$\eta = f\left(\frac{D_e}{D}, \frac{a}{D}, \frac{b}{D}, \frac{D_p}{D}, \frac{\rho_p}{\rho_g}, Re, Stk\right) \quad (7)$$

where, D, D_e, a, b are the geometrical parameters quoted in Figure 2. Re is the cyclone Reynolds number and Stk is the particle Stokes number. It should be mentioned that not all the cyclone geometrical parameters have the same influence on the collection efficiency. Hsiao et al. [49], Kenny et al. [50] found through sensitivity analyses that the vortex finder diameter D_e, inlet height a and width b have the strongest influence therefore, they were selected here as parameters to define the cyclone collection efficiency. Accordingly, the network structure was simplified instead of considering all the geometrical parameters. The cyclone Reynolds number and particle Stokes number are defined as:

$$Re = \frac{\rho v_{ig} D}{\mu} \qquad Stk = \frac{\rho_p D_p^2 v_{ig} C_c}{18 \mu D} \quad (8)$$

where, ρ_p is the particle mass density, D_p is the particle diameter, v_{ig} is the gas velocity at the cyclone inlet, μ is the gas dynamic viscosity and C_c is the Cunningham correction factor. The dataset employed for the training and testing of the ANN was derived from the experimental works of [19,51–62]. The dataset comprises 981 samples of collection efficiency values from 25 different cyclone designs, whose are reported in Table 1. The geometrical variables and process parameters span wide ranges of values, which make the dataset appropriate for the model training, validation and testing.

Table 1. Dimensionless geometrical and process parameters of experimental cyclones used for the training of the BPNN.

D [m]	D_e/D	a/D	b/D	D_p/D (10^{-4})	ρ_p/ρ_g	Re (10^5)	Stk (10^{-2})
0.9	0.3	0.5	0.3	0.017–0.16	2208	7.577	0.029–2.38
0.0219	0.36	0.58	0.32	2–4.4	816	0.023–0.05	0.437–2.15
0.0219	0.45	0.58	0.32	3–4.2	816	0.023–0.05	1.016–2.93
0.0219	0.62	0.58	0.32	2.6–4.3	816	0.033–0.05	1.114–3.29
0.0219	0.79	0.58	0.32	3.5–4.5	816	0.033–0.05	1.946–3.80
0.0311	0.25	0.41	0.22	1.3–2.7	816	0.034–0.071	0.230–1.55
0.0311	0.32	0.41	0.22	1.3–2.7	816	0.034–0.071	0.249–1.72
0.0311	0.43	0.41	0.22	1.3–3	816	0.034–0.071	0.333–2.07
0.0311	0.56	0.41	0.22	2–3	816	0.034–0.071	0.504–2.06
0.0411	0.24	0.31	0.17	1–2.34	816	0.034–0.071	0.275–2.41
0.25	0.5	0.5	0.2	0.52–2.82	730	1.24–3.76	0.031–1.18
0.25	0.5	0.5	0.3	0.52–2.82	730	1.679	0.020–0.52
0.25	0.5	0.75	0.2	0.52–2.82	730	1.679	0.020–0.52
0.25	0.5	0.5	0.1	0.52–2.82	730	5.038	0.062–1.58
0.25	0.5	0.25	0.2	0.52–2.82	730	5.038	0.062–1.58
0.25	0.3	0.5	0.2	0.52–2.82	730	2.519	0.031–0.79
0.4	0.5	0.5	0.2	0.02–0.15	2250	2.92	0.024–0.8
0.15	0.23	0.53	0.13	0.06–0.26	2208	1.04	0.061–0.66
0.03	0.49	0.4	0.2	0.25–0.73	875	0.272–0.498	0.095–1.73
0.031	0.5	0.4	0.16	0.16–2.6	875	0.167–0.334	0.026–9.33
0.072	0.44	0.5	0.23	0.12–0.31	2416	0.83–1.07	0.18–1.54
0.03	0.5	0.4	0.2	0.16–1	875	0.23	0.034–1.27
0.076	0.5	0.46	0.19	0.04–1.3	3290	0.4–1.01	0.015–10.2
0.186	0.43	0.72	0.36	0.02–0.71	2250	2.47	0.017–9.6
0.072	0.44	0.47	0.12	0.1–0.53	1916	0.525–0.859	0.064–6.03

2.6. Dataset for BPNN Validation and Comparison with Existing Methods

The meta-model of the cyclone has been validated with a set of experimental data from the empirical works of Hoffmann et al. [6], Obermair & Staudinger [63], Beeckmans & Kim [64], Iozia & Leith [10], Zhang [65], Dirgo & Leith [66], Zhao [60]. This set of data is composed by the experimental values of collection efficiencies for different cyclone designs, which are reported in Table 2.

Table 2. Parameters of experimental cyclones of Hoffman et al. (**1**), Obermair & Staudinger (**2**), Beeckmans & Kim (**3**), Iozia et al. (**4**), Zhang (**5**), Dirgo (**6**), Zhao (**7**) used for the meta-model validation.

N°	D [m]	D_e/D	a/D	b/D	D_p/D (10^{-4})	ρ_p/ρ_g	Re (10^5)	Stk (10^{-3})
1	0.2	0.375	0.5	0.2	0.05–0.25	2275	2.486	0.45–10.6
2	0.4	0.375	0.44	0.25	0.03–0.22	2308	3.341	0.39–21.8
3	0.152	0.5	0.542	0.25	0.04–0.31	1183	1.229	0.14–7.8
4	0.25	0.5	0.5	0.2	0.05–0.27	730	2.519	0.28–7.8
5	0.3	0.5	0.5	0.2	0.033–0.21	2250	2.39	0.35–1.3
6	0.305	0.5	0.5	0.2	0.045–0.19	725	2.022	0.17–3.1
7	0.3	0.5	0.5	0.2	0.001–0.22	2250	4.013	0.003–26.2

2.7. Classical Models to Predict Collection Efficiency

Four different classic semi-empirical models are utilized for comparison with the present meta-model. They are briefly described in the following 4 items.

1. Iozia et al. [8] calculated the grade-efficiency curve from the particle cut-off diameter d_{50} (Equation (9)) from the regression of experimental data (β is a fitting coefficient [17]).

$$d_{50} = \sqrt{\frac{9\mu Q}{\pi(H-S)\rho_p V_{tmax}^2}} \qquad \eta(D_p) = \frac{1}{1+\left(\frac{d_{50}}{D_p}\right)^{\beta}} \tag{9}$$

2. Clift et al. [11] (Equation (10)) proposed the following equation to find the cyclone collection efficiency from the particle residence time inside the cyclone body (t_{res}):

$$\eta(D_p) = 1 - \exp\left[-\frac{\rho_p}{9\mu}(D_p t_c)^2 t_{res}\right] \tag{10}$$

where, t_c is the characteristic cyclone time which is the ratio between the tangential velocity at the inlet of the cyclone and the cylindrical body radius.

3. Mothes et al. [13] developed a relation for the dust collection efficiency considering the particle transportation physics due to the gas motion, centrifugal and drag forces [53]:

$$\eta(D_p) = 1 - \left(\frac{m_1 - C_1}{C_2}\right) \times \exp\left[-\frac{\frac{2\pi D}{2} w\left(S - \frac{a}{2}\right)}{Q}\right] \tag{11}$$

where, m_1, C_1, C_2 are model's parameters, w is the mean radial velocity of the particles, Q is the cyclone inlet gas flow rate.

4. Li & Wang [14] derived the removal efficiency of the cyclone from the distribution of the particles concentration inside the cyclone body.

$$\eta(D_p) = 1 - \exp(-\lambda\theta_1) \tag{12}$$

where λ is a function of Stk, re-entrainment coefficient, radial particle velocity and radial turbulent diffusion coefficient, and θ_1 is the average angular position of the particle inside the cyclone body.

For further insights on the definitions of the above relations, see the article of Marinos et al. [67].

Only one statistical model based on the multi-linear regression approach was compared to the present meta-model. Zhao [18] developed a predicting logistic equation considering the dimensionless cyclone parameters and particles properties $D_e, a/D, b/D, Re, Stk$. The final equation obtained for the particles collection efficiency is reported as follows:

$$\eta(D_p) = 1/\left\{1 + \exp\left[-\left(\alpha_0 + \alpha_1 \ln\left[\frac{(a \cdot b)}{D_e^2}\right] + \alpha_2 \ln(Re) + \alpha_3 \ln(Stk)\right)\right]\right\} \tag{13}$$

where the regression coefficients $\alpha_0, \alpha_1, \alpha_2, \alpha_3$ were derived on the base of the experimental data from Iozia et al. [19] through a stepwise multiple regression algorithm and set equal to −7, 1.25, 0.61 and 2.09, respectively.

3. Results and Discussion

In this Section the results of the training and testing of the models are presented and discussed. The comparison between the prediction capabilities of the present models with the experimental data and the other alternative models is presented.

3.1. BPNN Training and Testing

Table 3 shows various combinations of the training batch size, n° of epochs, activation function and optimization algorithm hyperparameters and the corresponding MTE, MVE and MTA obtained in the various BPNN training steps. As mentioned in Section 2.2, the criteria to select the best combination of parameters was to minimise the MTE and MVE and

maximise the MTA. Results show that the achieved MTE, MVE and MTA in training ID 5 (bold highlighted) are the most satisfactory. The training 5 exhibits a consistent reduction in both training and validation losses compared to others suggesting a well-generalized model, as there is no evident divergence between the two loss curves and so there was no overfitting during the training process. Based on these results, the BPNN with these hyperparameters was selected as the final model for predicting the cyclone collection efficiency. Figure 4 shows the values of the train and validation loss as a function of the n° of epochs for the selected combination of hyperparameters.

Table 3. MTE, MVE and MTA for various combinations of BPNN hyperparameters.

Training ID	Batch Size	Epochs	Optim. Algorithm	Act. Function	MTE [%]	MVE [%]	MTA [%]
1	5	90	Adam	ReLu	3.47	2.97	87.7
2	5	90	Adam	Sigmoid	6.23	6.6	83.3
3	5	90	Adagrad	Relu	12.1	12.3	72.7
4	5	90	Adagrad	Sigmoid	17.9	17.3	66.6
5	**5**	**100**	**Adam**	**ReLu**	**2.66**	**2.87**	**89.8**
6	5	100	Adam	Sigmoid	6.22	6.43	79.5
7	5	100	Adagrad	ReLu	14.3	14.5	73.5
8	5	100	Adagrad	Sigmoid	12.4	12.6	67.2
9	15	90	Adam	ReLu	3.87	3.39	87.9
10	15	90	Adam	Sigmoid	7.48	7	81
11	15	90	Adagrad	ReLu	13.9	13.9	70.3
12	15	90	Adagrad	Sigmoid	20.4	19.6	66.4
13	15	100	Adam	ReLu	3.59	2.94	85.7
14	15	100	Adam	Sigmoid	7.16	7.24	81.5
15	15	100	Adagrad	ReLu	19.7	19.9	71.6
16	15	100	Adagrad	Sigmoid	15.7	15.5	66.8

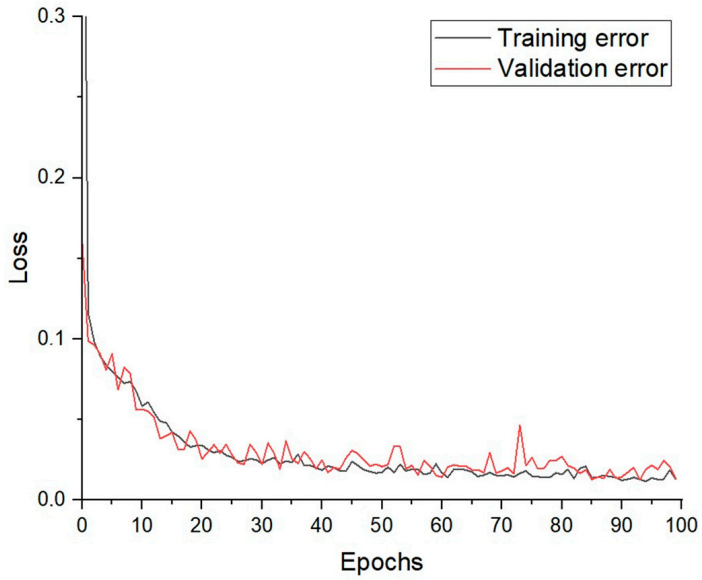

Figure 4. Train and validation loss against number of epochs.

3.2. SVR Training and Testing

Table 4 shows different combinations of kernel function, regularization parameter C and epsilon ε used for the training of the SVR. The combination of hyperparameters that given the lowest MTE and highest MTA during training and testing was chosen for the final SVR model structure. This has been achieved with training 4 hyperparameters combination, therefore the corresponding parameters were chosen for the final SVR model.

Table 4. MTE and MTA for various combinations of SVR hyperparameters.

Training ID	Kernel Function	C	ε	MTE [%]	MTA [%]
1	linear	0.1	0.01	8.9	69
2	polynomial	1	0.01	8.4	73.8
3	RBF	10	0.1	2.9	85.6
4	**RBF**	**100**	**0.01**	**1.7**	**89.8**
5	sigmoid	10	0.1	8.7	69.5
6	polynomial	100	0.2	5.3	80
7	RBF	10	0.2	3.2	84.5
8	polynomial	10	0.2	5.9	77.9
9	RBF	0.1	0.5	12.4	64.7
10	polynomial	0.1	0.2	8.2	73.3

3.3. BPNN and SVR Validation and Comparison with Classical Models

The present BPNN model was validated againts experimental data from the literature (see Section 2.6) and the predictions have been compared with those of classical models. Table 5 compares the mean squared error between the predictions of the present BPNN and the considered semi-empirical and statistical models against the experimental measurements of the validation dataset. The obtained mean squared error of the BPNN is equal to or less than 0.008 for 5 out of 7 experimental cases. The present BPNN model appears to have a lower overall mean squared error than all the classical methods. The best performance was obtained with the experimental cyclone **1**, while the worst is obtained with the cyclone **6**. Compared to the semi-empirical models of Clift et al. [13], Li & Wang [16] and Iozia et al. [10], the present BPNN model gives significantly better predictions with an improvement between the 71% and 96%. The model of Mothes et al. [15] gives good predictions of the particle collection efficiency of the tested cyclones (mean squared error < 0.028). It provides better previsions than the present BPNN for cyclones **2** and **5**. On the other hand, the BPNN model performs better with the cyclones **1**, **4** and **7**. Compared to the statistical model of Zhao [18], the present model gives better predictions for cyclones **1**, **2**, **3** and **4**, comparable predictions for **4** and **7** and worse predictions for **5**. This comparison proved that the ability to capture non-linear relationships between the input-output variables of the present BPNN plays a key role in the predictions' accuracy of the collection efficiency curve. In fact, the multi-linear regression model of Zhao [18], has an overall mean squared error which is 1.85 times higher than that of the BPNN model (see Diff on Table 5). Moreover, the BPNN model shows better predictions of Zhang [65] CFD model for the cyclone **5**, with a mean squared error of 0.013 against the 0.023, respectively.

Table 5. Mean squared error of predictions for all particles' diameters for Hoffman et al. (**1**), Obermair & Staudinger (**2**), Beeckmans & Kim (**3**), Iozia et al. (**4**), Zhang (**5**), Dirgo (**6**), Zhao (**7**) experimental data.

	1	**2**	**3**	**4**	**5**	**6**	**7**	**Overall**	**Diff**
Present BPNN	0.001	0.008	0.006	0.006	0.013	0.017	0.003	0.007	1
Present SVR	0.0139	0.011	0.044	0.008	0.007	0.018	0.007	0.015	2.1
Clift et al. [13]	0.204	0.218	0.103	0.145	0.233	0.090	0.118	0.158	22.6
Li & Wang [16]	0.132	0.160	0.045	0.019	0.028	0.016	0.009	0.058	8.3
Zhao [18]	0.022	0.016	0.027	0.011	0.005	0.012	0.001	0.013	1.85
Mothes et al. [15]	0.009	0.003	0.005	0.028	0.005	0.017	0.007	0.011	1.6
Iozia et al. [10]	0.016	0.033	0.038	0.027	0.008	0.005	0.008	0.020	2.85

A comparison has been conducted between the prediction capabilities of the present SVR model and those of the present BPNN and classical models. In general, the SVR model yielded good predictions of the experimental data, with an overall MSE that is lower than those of Clift et al. [13], Li & Wang [16] and Iozia et al. [10] models, and comparable with the models of Zhao [18] and Mothes et al. [15]. However, SVR model provided worse

predictions in comparison to the BPNN model, with an obtained overall MSE that is more than 2 times higher than that of BPNN. Indeed, the SVR model exhibited higher prediction errors for almost all the experimental cyclones with the exception of cyclone **5**, for which it returned an MSE that was 54% lower than that of the BPNN model.

Generally, the collection efficiency of cyclones reduces significantly for particles with smaller diameters, as they are the most critical to be separated from the air flow. Accordingly, the overall performance of a cyclone at different operating conditions is strongly dependent to the collection of small diameter particles. To provide further insights, the comparison between the predictions of the present BPNN and SVR and classical models was carried out for particles diameters for which the experimental data show an efficiency lower than 50%. Table 6 shows that, for small particle diameter ranges, the present BPNN has better prediction capabilities compared to SVR and all the classical models. In particular, the model achieved an overall mean squared error between 3 and 20 times (see Diff in Table 6) lower than those of the classical models. The SVR model demonstrates better prediction capability for small particles in comparison to all the classical models, a part for the Mothes et al. [15] model which yielded lower overall MSE.

Table 6. Mean squared error of predictions for particles with small diameters for Hoffman et al. (**1**), Obermair & Staudinger (**2**), Beeckmans & Kim (**3**), Iozia et al. (**4**), Zhang (**5**), Dirgo (**6**), Zhao (**7**) experimental data.

	1	**2**	**3**	**4**	**5**	**6**	**7**	**Overall Small Dp**	**Diff**
Present BPNN	0.001	0.009	0.003	0.002	0.003	0.002	0.002	0.003	1
Present SVR	0.0183	0.016	0.027	0.001	0.011	0.015	0.014	0.014	4.6
Clift et al. [13]	0.132	0.137	0.065	0.014	0.054	0.005	0.027	0.062	20.6
Li & Wang [16]	0.166	0.100	0.034	0.014	0.005	0.006	0.014	0.048	16
Zhao [18]	0.072	0.057	0.027	0.005	0.005	0.003	0.028	0.028	9.3
Mothes et al. [15]	0.003	0.007	0.019	0.001	0.005	0.001	0.026	0.009	3
Iozia et al. [10]	0.060	0.170	0.051	0.002	0.015	0.001	0.03	0.047	15.6

The reported results can be visualized by comparing the collection efficiency curves predicted by the present BPNN and SVR models with those of the semi-empirical and statistical models from the literature, as shown in Figure 5a–g.

In predicting the collection efficiency curves of experimental data **1**, **3**, **4**, **7**, the present BPNN model demonstrated superior performance compared to the classical models. This is proved by the well superposition of the predicted curves by the BPNN model with the experimental efficiency curves, which reflect the low values of mean squared errors achieved by the model predictions. What distinguishes the present BPNN model from all the classical models is the flexibility in the generation of the collection efficiency curve, which is not constrained to a single mathematical function as in the semi-empirical or multilinear regression approaches. This is clearly shown with cyclone **3**, where the classical models predict the experimental collection efficiency curve through a logistic function that is far from the actual trend of the experimental values. On the other hand, the predictions of the BPNN model well fit the experimental data showing a very low mean squared error. Even when the experimental data follow a logistic function, the present BPNN model demonstrated good predictive capabilities (see as example Figure 5g). The curves represented in Figure 5a,e,g clearly show the superiority of the present BPNN model in the prediction of cyclones' collection efficiencies for smaller particles, representing the low mean squared errors obtained in the predictions (see Table 6). This appears to be fundamental in practical applications, where the overestimation of the collection efficiencies of the particles with smaller sizes can lead to unproper design of cyclones.

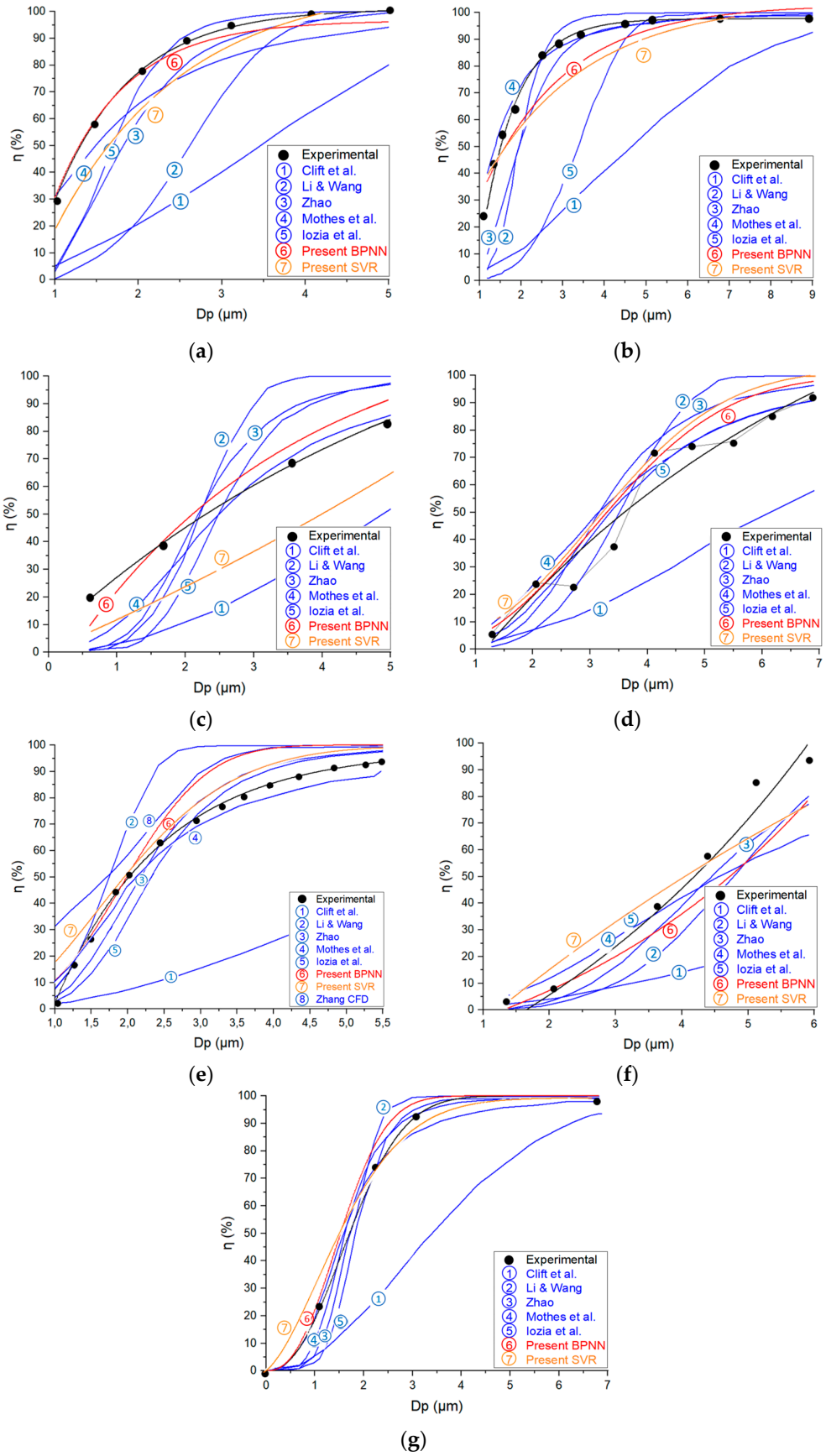

Figure 5. Predicted collection efficiency for Hoffman et al. (**a**), Obermair & Staudinger (**b**), Beeckmans & Kims (**c**), Iozia et al. (**d**), Zhang (**e**), Dirgo (**f**), Zhao (**g**) experimental data.

The present SVR model shows good predictions of the collection efficiency curves of the experimental cyclones. In the majority of cases, the SVR model is more effective than semi-empirical and statistical models in forecasting the collection efficiency curve. Nevertheless, the SVR model demonstrated lower performance in comparison to the BPNN model. Particularly, this can be observed by comparing the predicted efficiency curves of cyclones **1**, **3**, **7**. The superiority of the BPNN model compared to the SVR model can be attributed to several factors. The deep layered structure of the BPNN enables it to learn more effectively the non-linear relationships between input and output data of experimental cyclones in comparison to SVR. Accordingly, the BPNN model can easily adapt to the high variability of cyclones experimental data by adjusting the weights and biases of the hidden nodes during the iterative training procedure. While the SVR approach is capable of handling non-linearity and variability, it is less flexible than the BPNN due to its restriction to the regression function that interpolates the data in the high-dimensional space.

4. Conclusions

Cyclone separators play a vital role in numerous industries, e.g., in waste treatment and recycling plants, for dust collection or abatement purposes. However, predicting the efficiency of dust collection is challenging due to the complex physical phenomena involved in particle removal. This paper presents two models of cyclone separator for the prediction of the dust collection efficiency curve based on two machine-learning approaches: (i) back-propagation artificial neural network (BPNN), and (ii) support vector regression (SVR). After appropriate training and validation with experimental data taken from the literature, the models predictions have been compared with those obtained from semi-empirical and statistical methods suggested in the literature.

The comparison demonstrates that:

- The BPNN model is the best performing model, showing an improvement of the predictions capabilities between 40% and 90% compared to the other models. Only the semi-empirical model of Mothes et al. achieved results comparable to those obtained with the present BPNN.
- The SVR model yielded better predictions than the semi-empirical and statistical approaches. However, it demonstrated to be less performing than the BPNN model.
- Focusing on the efficiency predicting capabilities related to small particles only, the BPNN model showed an overall mean squared error that is between 2 and 20 times lower than that all the other models.

The present work provides two ML-based models, BPNN and SVR, that satisfactorily predicts the dust collection efficiency curve of the cyclone separator (overall MSE 0.007 and 0.015, respectively). It shares with the scientific community: (i) the weight and biases allowing to easily use the BPNN as a powerful tool for this specific application, (ii) the datasets and script of the codes used to train and validate the models, both BPNN and SVR, to allows other researchers to replicate and use them. Even though the developed models performed better than the semi-empirical ones, the results reported in this paper encourage further research in the improvements of this kind of meta-models. As reported in Section 2.5, the dimensionless variables considered in the meta-model did not explicitly account for some important phenomena occurring during the cyclone operation, such as the effect of solid load and particle agglomeration. Another limitation of the present BPNN and SVR models is that they have been trained and tested with data from laboratory scale cyclones, which operation can be different from the industrial ones. Future work will be devoted to include appropriate variables into the models and try further increasing their prediction capabilities by collecting data for training from cyclones of industrial plants.

Supplementary Materials: The following supporting information can be downloaded at: https://www.mdpi.com/article/10.3390/waste2030014/s1, The files containing the weight and biases resulted from the training of the BPNN and the dataset used for the training, validation and testing of the BPNN and SVR models.

Author Contributions: Conceptualization, E.B.; methodology, E.B.; software, E.B.; validation, E.B.; formal analysis, E.B.; investigation, E.B.; resources, E.B.; data curation, E.B.; writing—original draft preparation, E.B.; writing—review and editing, P.D. and M.M.; visualization, P.D. and M.M.; supervision, P.D. and M.M.; project administration, P.D. and M.M.; funding acquisition, P.D. and M.M. All authors have read and agreed to the published version of the manuscript.

Funding: The research work has been funded by Danieli S.p.A. and University of Padua (funding grant number 144923).

Institutional Review Board Statement: Not applicable.

Informed Consent Statement: Informed consent was obtained from all subjects involved in the study.

Data Availability Statement: The original contributions presented in the study are included in the article/Supplementary Materials, further inquiries can be directed to the corresponding author/s.

Conflicts of Interest: The authors declare no conflict of interest. The sponsors had no role in the design, execution, interpretation, or writing of the study.

Nomenclature

a	cyclone inlet height [m]
b	cyclone inlet width [m]
b_{ij}	ANN linear function bias
B	cyclone dust-outlet diameter [m]
C_1, C_2	cyclone dimensionless parameters
d_{50}	particle cut-off diameter [m]
D	cyclone diameter [m]
D_p	particle diameter [m]
D_{pmax}	maximum particle diameter [m]
M_{in}	mass of particles that enters the cyclone [kg]
M_{out}	mass of successfully separated particles [kg]
h	cyclone cylindrical body height [m]
H	cyclone total height [m]
Q	cyclone inlet volumetric flow rate [m^3/s]
Re	cyclone Reynolds number
S	cyclone vortex finder height [m]
Stk	particle Stokes number
t_c	cyclone characteristic time [s]
t_{res}	particle residence time inside cyclone body [s]
v_t	gas tangential velocity inside cyclone body [m/s]
w	particle mean radial velocity [m/s]
w_{ij}	BPNN weight
X_i	BPNN input layer node
Y_i	BPNN output layer node
z_{ij}	BPNN hidden layer output
ρ_p	particle mass density [kg/m^3]
ρ	air mass density [kg/m^3]
λ	cyclone efficiency parameter
μ	gas dynamic viscosity [Pa·s]
θ_1	particle average angular position inside cyclone body [°]

References

1. Bhasker, C. Flow simulation in industrial cyclone separator. *Adv. Eng. Softw.* **2010**, *41*, 220–228. [CrossRef]
2. Kashani, E.; Mohebbi, A.; Heidari, M.G. CFD simulation of the preheater cyclone of a cement plant and the optimization of its performance using a combination of the design of experiment and multi-gene genetic programming. *Powder Technol.* **2018**, *327*, 430–441. [CrossRef]
3. Frolov, S.M.; Smetanyuk, V.A.; Silantiev, A.S.; Sadykov, I.A.; Frolov, F.S.; Hasiak, J.K.; Shiryaev, A.A.; Sitnikov, V.E. Thermo-Mechano-Chemical Processing of Printed Circuit Boards for Organic Fraction Removal. *Waste* **2024**, *2*, 153–168. [CrossRef]
4. Shepherd, C.B.; Lapple, C.E. Flow pattern and pressure drop in cyclone dust collectors cyclone without intel vane. *Ind. Eng. Chem.* **1940**, *32*, 1246–1248. [CrossRef]
5. Lapple, C.E.; Shepherd1, C.B. Calculation of Particle Trajectories. *Ind. Eng. Chem.* **1940**, *32*, 605–617. [CrossRef]
6. Hoffmann, A.C.; Stein, L.E. Gas Cyclones and Swirl Tubes: Principles, Design and Operation. *Appl. Mech. Rev.* **2003**, *56*, B28–B29. [CrossRef]
7. Fayed, M.E.; Otten, L. *Handbook of Powder Science and Technology*; Springer Science & Business Media: Berlin/Heidelberg, Germany, 1997.
8. Stairmand, C.J. The design and performance of cyclone separators. *Trans. Instn. Chem. Engrs.* **1951**, *29*, 356–383.
9. Barth, W. Design and layout of the cyclone separator on the basis of new investigations. *Brenn. Warme Kraft* **1956**, *8*, 9.
10. Iozia, D.L.; Leith, D. Effect of cyclone dimensions on gas flow pattern and collection efficiency. *Aerosol Sci. Technol.* **1989**, *10*, 491–500. [CrossRef]
11. Lapple, C.E. Gravity and Centrifugal Separation. *Am. Ind. Hyg. Assoc. Q.* **1950**, *11*, 40–48. [CrossRef]
12. Leith, D. The collection efficiency of cyclone type particle collectors—A new theoretical approach. *AIChE Symp. Ser.* **1972**, *68*, 196–206.
13. Clift, R.; Ghadiri, M. A Critique of Two Models for Cyclone Performance. *AIChE J.* **1991**, *37*, 285–289. [CrossRef]
14. Dietz, P.W. Collection efficiency of cyclone separators. *AIChE J.* **1981**, *27*, 888–892. [CrossRef]
15. Mothes, H. Prediction removal in cyclone separators. *Int. Chem. Engng.* **1988**, *28*, 231–240.
16. Enliang, L.; Yingmin, W. A New Collection Theory of Cyclone Separators. *AIChE J.* **1989**, *35*, 666–669. [CrossRef]
17. Mumcu, A.G.; Avci, A. Parametric and General Evaluation of Mathematical Models Used for Critical Diameter Determination in Cyclone Separators. *Separations* **2023**, *10*, 284. [CrossRef]
18. Zhao, B. Development of a dimensionless logistic model for predicting cyclone separation efficiency. *Aerosol Sci. Technol.* **2010**, *44*, 1105–1112. [CrossRef]
19. Leith, D. The logistic function and cyclone fractional efficiency. *Aerosol Sci. Technol.* **1990**, *12*, 598–606. [CrossRef]
20. Wang, S.; Li, H.; Wang, R.; Wang, X.; Tian, R.; Sun, Q. Effect of the inlet angle on the performance of a cyclone separator using CFD-DEM. *Adv. Powder Technol.* **2019**, *30*, 227–239. [CrossRef]
21. Mirzaei, M.; Jensen, P.A.; Nakhaei, M.; Wu, H.; Zakrzewski, S.; Zhou, H.; Lin, W. CFD-DDPM coupled with an agglomeration model for simulation of highly loaded large-scale cyclones: Sensitivity analysis of sub-models and model parameters. *Powder Technol.* **2023**, *413*, 118036. [CrossRef]
22. Pandey, S.; Brar, L.S. On the performance of cyclone separators with different shapes of the conical section using CFD. *Powder Technol.* **2022**, *407*, 117629. [CrossRef]
23. Ijaz, M.; Farhan, M.; Farooq, M.; Moeenuddin, G.; Nawaz, S.; Soudagar, M.E.M.; Saqib, H.M.; Ali, Q. Numerical investigation of particles characteristics on cyclone performance for sustainable environment. *Part. Sci. Technol.* **2021**, *39*, 495–503. [CrossRef]
24. Nti, I.K.; Adekoya, A.F.; Weyori, B.A.; Nyarko-Boateng, O. Applications of artificial intelligence in engineering and manufacturing: A systematic review. *J. Intell. Manuf.* **2022**, *33*, 1581–1601. [CrossRef]
25. Islam, M.; Chen, G.; Jin, S. An Overview of Neural Network. *Am. J. Neural Netw. Appl.* **2019**, *5*, 7. [CrossRef]
26. Queiroz, L.H.; Santos, F.P.; Oliveira, J.P.; Souza, M.B. Physics-Informed deep learning to predict flow fields in cyclone separators. *Digit. Chem. Eng.* **2021**, *1*, 100002. [CrossRef]
27. Elsayed, K.; Lacor, C. Modeling, analysis and optimization of aircyclones using artificial neural network, response surface methodology and CFD simulation approaches. *Powder Technol.* **2011**, *212*, 115–133. [CrossRef]
28. Zhao, B.; Su, Y. Artificial neural network-based modeling of pressure drop coefficient for cyclone separators. *Chem. Eng. Res. Des.* **2010**, *88*, 606–613. [CrossRef]
29. Brar, L.S.; Elsayed, K. Analysis and optimization of multi-inlet gas cyclones using large eddy simulation and artificial neural network. *Powder Technol.* **2017**, *311*, 465–483. [CrossRef]
30. Elsayed, K.; Lacor, C. CFD modeling and multi-objective optimization of cyclone geometry using desirability function, Artificial neural networks and genetic algorithms. *Appl. Math. Model.* **2013**, *37*, 5680–5704. [CrossRef]
31. Le, D.K.; Yoon, J.Y. A hybrid CFD—Deep learning methodology for improving the accuracy of cut-off diameter prediction in coarse-grid simulations for cyclone separators. *Chem. Eng. Res. Des.* **2023**, *190*, 296–311. [CrossRef]
32. Tang, X.; Yue, Y.; Shen, Y. Prediction of separation efficiency in gas cyclones based on RSM and GA-BP: Effect of geometry designs. *Powder Technol.* **2023**, *416*, 118185. [CrossRef]
33. Zhao, B. Modeling pressure drop coefficient for cyclone separators: A support vector machine approach. *Chem. Eng. Sci.* **2009**, *64*, 4131–4136. [CrossRef]

34. Deng, Y.; Yu, B.; Sun, D. Multi-objective optimization of guide vanes for axial flow cyclone using CFD, SVM, and NSGA II algorithm. *Powder Technol.* **2020**, *373*, 637–646. [CrossRef]
35. Zhang, W.; Zhang, L.; Yang, J.; Hao, X.; Guan, G.; Gao, Z. An experimental modeling of cyclone separator efficiency with PCA-PSO-SVR algorithm. *Powder Technol.* **2019**, *347*, 114–124. [CrossRef]
36. Bülbül, M.A. Optimization of artificial neural network structure and hyperparameters in hybrid model by genetic algorithm: IOS–android application for breast cancer diagnosis/prediction. *J. Supercomput.* **2024**, *80*, 4533–4553. [CrossRef]
37. Konak, F.; Bülbül, M.A.; Türkoğlu, D. Feature Selection and Hyperparameters Optimization Employing a Hybrid Model Based on Genetic Algorithm and Artificial Neural Network: Forecasting Dividend Payout Ratio. *Comput. Econ.* **2024**, *63*, 1673–1693. [CrossRef]
38. Lillicrap, T.P.; Santoro, A.; Marris, L.; Akerman, C.J.; Hinton, G. Backpropagation and the brain. *Nat. Rev. Neurosci.* **2020**, *21*, 335–346. [CrossRef] [PubMed]
39. McCulloch, W.S.; Pitts, W. A logical calculus of the ideas immanent in nervous activity. *Bull. Math. Biophys.* **1943**, *5*, 115–133. [CrossRef]
40. Sharma, S.; Sharma, S.; Athaiya, A. Activation Functions in Neural Networks. *Int. J. Eng. Appl. Sci. Technol.* **2020**, *4*, 310–316. [CrossRef]
41. Belete, D.M.; Huchaiah, M.D. Grid search in hyperparameter optimization of machine learning models for prediction of HIV/AIDS test results. *Int. J. Comput. Appl.* **2022**, *44*, 875–886. [CrossRef]
42. Projects, L.; Sarang, P. *Artificial Neural Networks with Tensorflow 2*; Apress: Berkeley, CA, USA, 2021.
43. Awad, M.; Khanna, R. *Efficient Learning Machines*; Springer Nature: Berlin/Heidelberg, Germany, 2015; pp. 67–80.
44. Kavzoglu, T.; Colkesen, I. A kernel functions analysis for support vector machines for land cover classification. *Int. J. Appl. Earth Obs. Geoinf.* **2009**, *11*, 352–359. [CrossRef]
45. Oommen, T.; Misra, D.; Twarakavi, N.K.C.; Prakash, A.; Sahoo, B.; Bandopadhyay, S. An objective analysis of support vector machine based classification for remote sensing. *Math. Geosci.* **2008**, *40*, 409–424. [CrossRef]
46. Zhou, H.; Huang, S.; Zhang, P.; Ma, B.; Ma, P.; Feng, X. Prediction of jacking force using PSO-BPNN and PSO-SVR algorithm in curved pipe roof. *Tunn. Undergr. Sp. Technol.* **2023**, *138*, 105159. [CrossRef]
47. Zhao, G.; Wang, M.; Liang, W. A Comparative Study of SSA-BPNN, SSA-ENN, and SSA-SVR Models for Predicting the Thickness of an Excavation Damaged Zone around the Roadway in Rock. *Mathematics* **2022**, *10*, 1351. [CrossRef]
48. Sci Kit Learn. Available online: https://pypi.org/project/scikit-learn/ (accessed on 20 July 2023).
49. Hsiao, T.C.; Huang, S.H.; Hsu, C.W.; Chen, C.C.; Chang, P.K. Effects of the geometric configuration on cyclone performance. *J. Aerosol Sci.* **2015**, *86*, 1–12. [CrossRef]
50. Kenny, L.C.; Gussman, R.A. A direct approach to the design of cyclones for aerosol-monitoring applications. *J. Aerosol Sci.* **2000**, *31*, 1407–1420. [CrossRef]
51. Kim, J.C.; Lee, K.W. Experimental study of particle collection by small cyclones. *Aerosol Sci. Technol.* **1990**, *12*, 1003–1015. [CrossRef]
52. Xiang, R.; Park, S.H.; Lee, K.W. Effects of cone dimension on cyclone performance. *J. Aerosol Sci.* **2001**, *32*, 549–561. [CrossRef]
53. Ray, M.B.; Hoffmann, A.C.; Postma, R.S. Performance of different analytical methods in evaluating grade efficiency of centrifugal separators. *J. Aerosol Sci.* **2000**, *31*, 563–581. [CrossRef]
54. Bohnet, M. Influence of the gas temperature on the separation efficiency of aerocyclones. *Chem. Eng. Process.* **1995**, *34*, 151–156. [CrossRef]
55. Zhu, Y.; Lee, K.W. Experimental study on small cyclones operating at high flowrates. *J. Aerosol Sci.* **1999**, *30*, 1303–1315. [CrossRef]
56. Hoekstra, A.J. Gas Flow Field and Collection Efficiency of Cyclone Separators. Ph.D. Thesis, Delft University of Technology, Delft, The Netherlands, 2000; pp. 1–165.
57. Yoshida, H.; Kwan-Sik, Y.; Fukui, K.; Akiyama, S.; Taniguchi, S. Effect of apex cone height on particle classification performance of a cyclone separator. *Adv. Powder Technol.* **2003**, *14*, 263–278. [CrossRef]
58. Lim, K.S.; Kim, H.S.; Lee, K.W. Characteristics of the collection efficiency for a cyclone with different vortex finder shapes. *J. Aerosol Sci.* **2004**, *35*, 743–754. [CrossRef]
59. Kim, H.T.; Lee, K.W.; Kuhlman, M.R. Exploratory design modifications for enhancing cyclone performance. *J. Aerosol Sci.* **2001**, *32*, 1135–1146. [CrossRef]
60. Zhao, B. Development of a new method for evaluating cyclone efficiency. *Chem. Eng. Process. Process Intensif.* **2005**, *44*, 447–451. [CrossRef]
61. Yang, J.; Sun, G.; Gao, C. Effect of the inlet dimensions on the maximum-efficiency cyclone height. *Sep. Purif. Technol.* **2013**, *105*, 15–23. [CrossRef]
62. Huang, A.N.; Maeda, N.; Shibata, D.; Fukasawa, T.; Yoshida, H.; Kuo, H.P.; Fukui, K. Influence of a laminarizer at the inlet on the classification performance of a cyclone separator. *Sep. Purif. Technol.* **2017**, *174*, 408–416. [CrossRef]
63. Obermair, S.; Staudinger, G. The dust outlet of a gas cyclone and its effects on separation efficiency. *Chem. Eng. Technol.* **2001**, *24*, 1259–1263. [CrossRef]
64. Beeckmans, J.M.; Kim, C.J. Analysis of the efficiency of reverse flow cyclones. *Can. J. Chem. Eng.* **1977**, *55*, 640–643. [CrossRef]
65. Zhang, Z.W.; Li, Q.; Zhang, Y.H.; Wang, H.L. Simulation and experimental study of effect of vortex finder structural parameters on cyclone separator performance. *Sep. Purif. Technol.* **2022**, *286*, 120394. [CrossRef]

66. Dirgo, J.; Leith, D. Cyclone collection efficiency: Comparison of experimental results with theoretical predictions. *Aerosol Sci. Technol.* **1985**, *4*, 401–415. [CrossRef]
67. Marinos, C.; Economopoulou, A.A.; Economopoulos, A.P. Comparative Fractional Efficiency Predictions by Selected Cyclone Simulation Models. *J. Environ. Eng.* **2007**, *133*, 556–567. [CrossRef]